

Finite element approximations for near-incompressible and near-inextensible transversely isotropic bodies

F. Rasolofoson B.J. Grieshaber B.D. Reddy

Department of Mathematics and Applied Mathematics,
and Centre for Research in Computational and Applied Mechanics, University of Cape Town,
South Africa

(rslfar002@myuct.ac.za,beverley.grieshaber@uct.ac.za,daya.reddy@uct.ac.za)

Abstract

This work comprises a detailed theoretical and computational study of the boundary value problem for transversely isotropic linear elastic bodies. General conditions for well-posedness are derived in terms of the material parameters. The discrete form of the displacement problem is formulated for conforming finite element approximations. The error estimate reveals that anisotropy can play a role in minimizing or even eliminating locking behaviour, for moderate values of the ratio of Young's moduli in the fibre and transverse directions. In addition to the standard conforming approximation an alternative formulation, involving under-integration of the volumetric and extensional terms in the weak formulation, is considered. The latter is equivalent to either a mixed or a perturbed Lagrangian formulation, analogously to the well-known situation for the volumetric term. A set of numerical examples confirms the locking-free behaviour in the near-incompressible limit of the standard formulation with moderate anisotropy, with locking behaviour being clearly evident in the case of near-inextensibility. On the other hand, under-integration of the extensional term leads to extensional locking-free behaviour, with convergence at superlinear rates.

Keywords: solids, finite element methods, elasticity

1 Introduction

Anisotropy is a significant mechanical feature of composite materials, for example, in the aerospace and automotive industries. It occurs naturally in crystalline structures, geotechnical materials, and in the mechanical properties of biological media such as muscles, tendons, or bones (see for example [1, 2, 3, 4]). Fibrous or fibre-reinforced structures are generally modelled as transversely isotropic materials, with the plane normal to the fibre direction corresponding to a plane of isotropy. Important early contributions to the mechanics of fibre-reinforced materials include the works [5, 6, 7]. The monograph [8] gives a detailed presentation of the mechanics of anisotropic materials.

Early work on the linear problem, in addition to some of the works cited above, includes the investigations [9, 10] of uniqueness and local (pointwise) stability for materials with the constraint of inextensibility. There have been extensive theoretical and computational studies carried out of the behaviour of transversely isotropic materials, or the closely related topic of inextensible or near-inextensible materials, in the context of hyperelasticity (see for example the key works [11, 12, 13]). Mixed finite element approximations leading to stable formulations have been developed and implemented for near-incompressibility and near-inextensibility in [14], while transverse anisotropy has been studied, also using various mixed finite element formulations, in [15, 16]. A mixed approach allied with a Lagrange multiplier or perturbed Lagrange multiplier formulation of the inextensibility constraint forms the basis of a computational study in [17]. In earlier work, a corresponding numerical study, using a mixed three-field approach for the linear problem, has been carried out in [18]. The recent contribution [19] presents a locking-free implementation for nonlinear transversely isotropic elasticity, the inextensibility constraint in the fibre direction being accommodated using a perturbed Lagrangian formulation. A corresponding treatment of the small-strain problem has been the subject of [20], in which limiting extensibility is investigated numerically using penalty, Lagrange multiplier, and perturbed Lagrangian approaches.

A model of a bi-directional elastic composite has been developed in [21], and studied computationally for the case of plane deformations, as an extension of earlier work [22] on single families of fibres. The work [23] extends conventional studies of transverse isotropy by developing a model

in the context of nonlinear elasticity, in which the fibres are assumed to be resistant to flexure and twist, in addition to extension.

There has been little work on the well-posedness of problems with internal constraints such as inextensibility, in contrast to the many treatments of incompressibility. The investigation [24] approaches the problem via a mixed formulation of Hellinger-Reissner type, and establishes conditions on the elastic constants for the problem to be well-posed for inextensible materials, and also for the case of orthotropy. Corresponding abstract results have been presented in [25] for the case of non-homogeneous materials. In [2] conditions for pointwise stability are obtained for materials in plane strain.

The purpose of this work is to undertake a detailed theoretical and computational study of the behaviour of transversely isotropic linear elastic materials, with a view to establishing conditions under which conforming finite element approximations are uniformly convergent in the incompressible and inextensible limits. In this sense the present investigation extends considerably the work reported in [20], by first establishing conditions for well-posedness of the continuous problem, then by establishing error estimates for conforming finite element approximations that shed light on the conditions under which locking-free behaviour can be expected. It is shown that the presence of transverse isotropy leads to behaviour that is volumetrically locking-free, in circumstances that would lead to locking behaviour for isotropic materials. In particular, in situations of moderate anisotropy, when the ratio of Young's modulus in the fibre direction to that in the plane of isotropy is not too large, in a sense that will be made precise, volumetric locking-free behaviour results for low-order elements.

A second contribution relates to the circumstances under which extensional locking-free behaviour occurs for low-order elements. While the standard approximations do in fact exhibit locking, it is shown that, analogous to the now classical result for near-incompressibility [26], under-integration of the extensional term results in locking-free behaviour. This approach is shown to be equivalent to a mixed formulation, as in the case of incompressible behaviour, and also to a perturbed Lagrangian approach of the kind presented, for example, in [20].

The structure of the rest of this work is as follows. Section 2 sets out the details of constitutive relations for transversely isotropic linear elastic materials, and establishes conditions on the mate-

rial constants for pointwise stability. The weak form of the boundary-value problem is presented in Section 3, and conditions for well-posedness derived. Section 4 is concerned with conforming finite element approximations. The standard error estimate reveals the role played by anisotropy in mitigating locking behaviour in the incompressible limit. An alternative approximation, employing under-integration of the volumetric and extensional terms, is related to a mixed as well as a perturbed Lagrangian formulation. These various features are explored numerically in Section 5, through two sets of example problems. The work concludes with a summary of results and a discussion of open problems.

2 Transversely isotropic materials

For a transversely isotropic linearly elastic material with fibre direction given by the unit vector \mathbf{a} , the elasticity tensor is given by [27, 28]

$$\mathbb{C} = \lambda \mathbf{I} \otimes \mathbf{I} + 2\mu_t \mathbb{I} + \beta \mathbf{M} \otimes \mathbf{M} + \alpha(\mathbf{I} \otimes \mathbf{M} + \mathbf{M} \otimes \mathbf{I}) + \gamma \mathbb{M}. \quad (1)$$

Here \mathbf{I} is the second-order identity tensor, \mathbb{I} is the fourth-order identity tensor, $\mathbf{M} = \mathbf{a} \otimes \mathbf{a}$, and \mathbb{M} is the fourth-order tensor defined by

$$\mathbb{M}\mathbf{R} = \mathbf{M}\mathbf{R} + \mathbf{R}\mathbf{M} \quad \text{for any second-order tensor } \mathbf{R}. \quad (2)$$

λ denotes the first Lamé parameter, the shear modulus in the plane of isotropy is μ_t , μ_l is the shear modulus along the fibre direction, and

$$\gamma = 2(\mu_l - \mu_t). \quad (3)$$

The further material constants α and β do not have a direct interpretation, though it will be seen that $\beta \rightarrow \infty$ in the inextensible limit.

In component form, equation (1) becomes

$$\begin{aligned} \mathbb{C}_{ABCD} = & \lambda \delta_{AB} \delta_{CD} + 2\mu_t \delta_{AC} \delta_{BD} + \beta M_{AB} M_{CD} + \alpha (\delta_{AB} M_{CD} + M_{AB} \delta_{CD}) \\ & + 2(\mu_l - \mu_t) (\delta_{AC} M_{BD} + M_{AC} \delta_{BD}). \end{aligned} \quad (4)$$

The corresponding linear stress-strain relation for small deformations is then

$$\begin{aligned} \boldsymbol{\sigma} &= \mathbb{C} \boldsymbol{\varepsilon} \\ &= \lambda (\text{tr} \boldsymbol{\varepsilon}) \mathbf{I} + 2\mu_t \boldsymbol{\varepsilon} + \beta (\mathbf{M} : \boldsymbol{\varepsilon}) \mathbf{M} + \alpha ((\mathbf{M} : \boldsymbol{\varepsilon}) \mathbf{I} + (\text{tr} \boldsymbol{\varepsilon}) \mathbf{M}) + \gamma (\boldsymbol{\varepsilon} \mathbf{M} + \mathbf{M} \boldsymbol{\varepsilon}), \end{aligned} \quad (5)$$

in which $\boldsymbol{\sigma}$ and $\boldsymbol{\varepsilon}$ denote the stress and the infinitesimal strain tensors; $\text{tr} \boldsymbol{\varepsilon}$ denotes the trace of $\boldsymbol{\varepsilon}$, and $\mathbf{M} : \boldsymbol{\varepsilon} = \boldsymbol{\varepsilon} \mathbf{a} \cdot \mathbf{a}$, obtained from the definition of \mathbf{M} , gives the strain in the direction of \mathbf{a} . The special case of an isotropic material is recovered by setting $\alpha = \beta = 0$ and $\mu_l = \mu_t$.

For the particular case in which $\mathbf{a} = \mathbf{e}_3$, the stress-strain relationship can be written in matrix form as

$$\begin{pmatrix} \sigma_{11} \\ \sigma_{22} \\ \sigma_{33} \\ \sigma_{23} \\ \sigma_{13} \\ \sigma_{12} \end{pmatrix} = \begin{pmatrix} \lambda + 2\mu_t & \lambda & \lambda + \alpha & 0 & 0 & 0 \\ \lambda & \lambda + 2\mu_t & \lambda + \alpha & 0 & 0 & 0 \\ \lambda + \alpha & \lambda + \alpha & \lambda + 2\mu_t + \beta + 2\alpha + 2\gamma & 0 & 0 & 0 \\ 0 & 0 & 0 & \mu_l & 0 & 0 \\ 0 & 0 & 0 & 0 & \mu_l & 0 \\ 0 & 0 & 0 & 0 & 0 & \mu_t \end{pmatrix} \begin{pmatrix} \varepsilon_{11} \\ \varepsilon_{22} \\ \varepsilon_{33} \\ 2\varepsilon_{23} \\ 2\varepsilon_{13} \\ 2\varepsilon_{12} \end{pmatrix}. \quad (6)$$

2.1 The compliance tensor

It is also useful to have available the inverse of (5), and to find the compliance tensor \mathbb{S} corresponding to \mathbb{C} ; that is,

$$\boldsymbol{\varepsilon} = \mathbb{S} \boldsymbol{\sigma}. \quad (7)$$

We derive here an explicit form for \mathbb{S} , using an approach that is more direct than that in [27].

First, from (5),

$$\begin{pmatrix} \text{tr}\boldsymbol{\varepsilon} \\ \mathbf{M} : \boldsymbol{\varepsilon} \end{pmatrix} = \frac{1}{\mathcal{K}} \begin{pmatrix} 2\mu_t + \beta + \alpha + 2\gamma & -\beta - 3\alpha - 2\gamma \\ -\lambda - \alpha & 3\lambda + 2\mu_t + \alpha \end{pmatrix} \begin{pmatrix} \text{tr}\boldsymbol{\sigma} \\ \mathbf{M} : \boldsymbol{\sigma} \end{pmatrix}, \quad (8)$$

and

$$\boldsymbol{\varepsilon}\mathbf{M} = \frac{1}{2\mu_t + \gamma}(\boldsymbol{\sigma}\mathbf{M} - \mathbf{M}\boldsymbol{\sigma}) + \mathbf{M}\boldsymbol{\varepsilon}, \quad (9)$$

where

$$\mathcal{K} = 2(\lambda + \alpha)(\mu_t - \alpha) + 2(\lambda + \mu_t)(2\mu_t + \beta + \alpha + 2\gamma). \quad (10)$$

Substituting back into (5) and using $(\mu_t\mathbf{I} + \gamma\mathbf{M})^{-1} = \frac{1}{\mu_t(\mu_t + \gamma)}[(\mu_t + \gamma)\mathbf{I} - \gamma\mathbf{M}]$, equation (7) becomes

$$\begin{aligned} \boldsymbol{\varepsilon} = \frac{1}{2\mu_t(\mu_t + \gamma)} & \left[(\mu_t + \gamma)\boldsymbol{\sigma} - \gamma\mathbf{M}\boldsymbol{\sigma} - (\mu_t + \gamma)(A\lambda + C\alpha)(\text{tr}\boldsymbol{\sigma})\mathbf{I} \right. \\ & - [\mu_t(A\alpha + C\beta) - \gamma(A\lambda + C\alpha)](\text{tr}\boldsymbol{\sigma})\mathbf{M} \\ & - (\mu_t + \gamma)(B\lambda + D\alpha)\mathbf{I}(\mathbf{M} : \boldsymbol{\sigma}) - [\mu_t(B\alpha + D\beta) - \gamma(B\lambda + D\alpha)]\mathbf{M}(\mathbf{M} : \boldsymbol{\sigma}) \\ & \left. - \frac{\gamma(\mu_t + \gamma)}{2\mu_t + \gamma}(\boldsymbol{\sigma}\mathbf{M} - \mathbf{M}\boldsymbol{\sigma}) + \frac{\gamma^2}{2\mu_t + \gamma}(\mathbf{M}\boldsymbol{\sigma}\mathbf{M} - \mathbf{M}\boldsymbol{\sigma}) \right], \end{aligned}$$

where

$$A = \frac{2\mu_t + \beta + \alpha + 2\gamma}{\mathcal{K}}, \quad B = -\frac{\beta + 3\alpha + 2\gamma}{\mathcal{K}}, \quad C = -\frac{\lambda + \alpha}{\mathcal{K}} \quad \text{and} \quad D = \frac{3\lambda + 2\mu_t + \alpha}{\mathcal{K}}. \quad (11)$$

Next, we obtain expressions for the five material parameters in (5) in terms of five physically meaningful constants, viz. E_t : Young's modulus in the transverse direction; E_l : Young's modulus in the fibre direction; and ν_t and ν_l : respectively Poisson's ratios for the transverse strain with respect to the fibre direction and the plane normal to it. The remaining constants are the two

shear moduli μ_t and μ_l , and one may further define μ_t by

$$\mu_t = \frac{E_t}{2(1 + \nu_t)}. \quad (12)$$

Then, choosing the fibre direction to coincide with the basis vector e_3 , the compliance relation has the alternate form [2]

$$\begin{pmatrix} \varepsilon_{11} \\ \varepsilon_{22} \\ \varepsilon_{33} \\ 2\varepsilon_{23} \\ 2\varepsilon_{13} \\ 2\varepsilon_{12} \end{pmatrix} = \begin{pmatrix} \frac{1}{E_t} & -\frac{\nu_t}{E_t} & -\frac{\nu_l}{E_l} & 0 & 0 & 0 \\ -\frac{\nu_t}{E_t} & \frac{1}{E_t} & -\frac{\nu_l}{E_l} & 0 & 0 & 0 \\ -\frac{\nu_l}{E_l} & -\frac{\nu_l}{E_l} & \frac{1}{E_l} & 0 & 0 & 0 \\ 0 & 0 & 0 & \frac{1}{\mu_l} & 0 & 0 \\ 0 & 0 & 0 & 0 & \frac{1}{\mu_l} & 0 \\ 0 & 0 & 0 & 0 & 0 & \frac{1}{\mu_t} \end{pmatrix} \begin{pmatrix} \sigma_{11} \\ \sigma_{22} \\ \sigma_{33} \\ \sigma_{23} \\ \sigma_{13} \\ \sigma_{12} \end{pmatrix}. \quad (13)$$

The nature of the Poisson's ratios may be determined by considering some simple loading cases. For the case of uniaxial stress in the x_3 -direction, with $\mathbf{a} = e_3$, the strains are given by

$$\varepsilon_{11} = -\frac{\nu_l}{E_l}\sigma_{33}, \quad \varepsilon_{22} = -\frac{\nu_l}{E_l}\sigma_{33} \quad \text{and} \quad \varepsilon_{33} = \frac{\sigma_{33}}{E_l}. \quad (14)$$

Thus

$$\varepsilon_{11} = \varepsilon_{22} = -\nu_l\varepsilon_{33}, \quad (15)$$

so that ν_l determines the lateral contraction in the plane of isotropy, as a result of strain in the longitudinal or fibre direction.

Similarly, considering the case of uniaxial stress in the (transverse) x_1 -direction, we have

$$\varepsilon_{11} = \frac{\sigma_{11}}{E_t}, \quad \varepsilon_{22} = -\frac{\nu_t}{E_t}\sigma_{11}, \quad \text{and} \quad \varepsilon_{33} = -\frac{\nu_l}{E_l}\sigma_{11}, \quad (16)$$

so that

$$\varepsilon_{33} = -\nu_l\frac{E_t}{E_l}\varepsilon_{11}. \quad (17)$$

Thus, lateral contraction in the fibre direction depends directly on the ratio of Young's moduli in the fibre and transverse directions. In the inextensible limit, when $E_l/E_t \rightarrow \infty$, there is no lateral contraction in the fibre direction.

By inverting (13) and comparing with (6), the material parameters λ , α and β can be written in terms of the engineering constants as

$$\begin{aligned}\lambda &= \frac{E_t(\nu_l^2 E_t + \nu_t E_l)}{(1 + \nu_t)(E_l(1 - \nu_t) - 2\nu_l^2 E_t)}, \\ \alpha &= \frac{E_t [E_l \nu_l(1 + \nu_t) - \nu_l^2 E_t - \nu_t E_l]}{(1 + \nu_t)(E_l(1 - \nu_t) - 2\nu_l^2 E_t)}, \\ \beta &= \frac{E_l^2(1 - \nu_t^2) - E_t^2 \nu_l^2 + E_t E_l(1 - 2\nu_t \nu_l - 2\nu_l)}{(1 + \nu_t)(E_l(1 - \nu_t) - 2\nu_l^2 E_t)} - 4\mu_l.\end{aligned}\tag{18}$$

Henceforth, we set

$$E_l = pE_t \quad \text{and} \quad \mu_l = q\mu_t.\tag{19}$$

Thus p measures the stiffness in the fibre direction relative to that in the plane of isotropy, and q is the ratio of the two shear moduli. Using (19) the expressions (18) become

$$\mu_l = \frac{qE_t}{2(1 + \nu_t)},\tag{20a}$$

$$\lambda = \frac{(\nu_t p + \nu_l^2)}{(1 + \nu_t)((1 - \nu_t)p - 2\nu_l^2)} E_t,\tag{20b}$$

$$\alpha = \frac{(\nu_l - \nu_t + \nu_t \nu_l)p - \nu_l^2}{((1 + \nu_t)((1 - \nu_t)p - 2\nu_l^2)} E_t,\tag{20c}$$

$$\beta = \frac{(1 - \nu_t^2)p^2 + (-2\nu_t \nu_l + 2q\nu_t - 2\nu_l + 1 - 2q)p - (1 - 4q)\nu_l^2}{(1 + \nu_t)((1 - \nu_t)p - 2\nu_l^2)} E_t.\tag{20d}$$

2.2 Pointwise stability

The condition of strong convexity, or pointwise stability, is equivalent to the positive definiteness of the strain energy [29]: that is,

$$\varepsilon_{AB}\mathbb{C}_{ABCD}\varepsilon_{CD} > 0 \quad \text{for any non-zero second-order tensor } \varepsilon. \quad (21)$$

From (4) we have

$$\begin{aligned} \varepsilon_{AB}\mathbb{C}_{ABCD}\varepsilon_{CD} &= \lambda(\text{tr}\varepsilon)^2 + 2\mu_t(\varepsilon : \varepsilon) + \beta(\varepsilon : \mathbf{M})^2 + 2\alpha(\text{tr}\varepsilon)(\varepsilon : \mathbf{M}) + 2\gamma(\varepsilon : \varepsilon\mathbf{M}) \\ &= \left(\lambda + \frac{2}{3}\mu_t\right)(\text{tr}\varepsilon)^2 + 2\mu_t|\text{dev}\varepsilon|^2 + \beta(\varepsilon : \mathbf{M})^2 \\ &\quad + 2\alpha(\text{tr}\varepsilon)(\varepsilon : \mathbf{M}) + 2\gamma(\varepsilon : \varepsilon\mathbf{M}). \end{aligned}$$

Here $\text{dev}\varepsilon = \varepsilon - (1/3)(\text{tr}\varepsilon)\mathbf{I}$ is the deviatoric part of the strain. We assume that

$$E_t, E_l > 0, \quad \text{giving } p > 0, \quad (22)$$

we further assume that

$$\mu_l \geq \mu_t > 0, \quad \text{implying } \gamma \geq 0 \quad (23)$$

and from equation (12), $\nu_t > -1$.

We note that $\varepsilon : \mathbf{M} = \varepsilon\mathbf{a} \cdot \mathbf{a}$ and $\varepsilon : \varepsilon\mathbf{M} = |\varepsilon\mathbf{a}|^2$, with $|\varepsilon\mathbf{a}|^2 \geq (\varepsilon\mathbf{a} \cdot \mathbf{a})^2$, then

$$\begin{aligned} \varepsilon_{AB}\mathbb{C}_{ABCD}\varepsilon_{CD} &\geq \left(\lambda + \frac{2}{3}\mu_t\right)(\text{tr}\varepsilon)^2 + (\beta + 2\gamma)(\varepsilon\mathbf{a} \cdot \mathbf{a})^2 + 2\alpha(\text{tr}\varepsilon)(\varepsilon\mathbf{a} \cdot \mathbf{a}) \\ &\quad + 2\mu_t|\text{dev}\varepsilon|^2. \end{aligned} \quad (24)$$

We can obtain the pointwise stability condition by establishing conditions such that the right hand side of the inequality (24) is strictly positive; that is $\mathcal{A} + 2\mu_t|\text{dev}\varepsilon|^2 > 0$, with

$$\mathcal{A} = \left(\lambda + \frac{2}{3}\mu_t\right)(\text{tr}\varepsilon)^2 + (\beta + 2\gamma)(\varepsilon\mathbf{a} \cdot \mathbf{a})^2 + 2\alpha(\text{tr}\varepsilon)(\varepsilon\mathbf{a} \cdot \mathbf{a}). \quad (25)$$

The discriminant of \mathcal{A} , treated as a quadratic function of $\text{tr}\varepsilon$ and $\varepsilon\mathbf{a} \cdot \mathbf{a}$, is

$$\Delta = 4 \left[\alpha^2 - \left(\lambda + \frac{2}{3}\mu_t \right) (\beta + 2\gamma) \right] \quad (26)$$

We assume that

$$\lambda + \frac{2}{3}\mu_t > 0, \quad (27)$$

so that if $\Delta < 0$, then $\mathcal{A} > 0$ and we have pointwise stability.

We have

$$\lambda + \frac{2}{3}\mu_t = \frac{(2\nu_t + 1)p + \nu_t^2}{3(1 + \nu_t)[(1 - \nu_t)p - 2\nu_t^2]} E_t > 0, \quad (28)$$

which is true iff

$$\begin{cases} (2\nu_t + 1)p + \nu_t^2 > 0 \text{ and } (1 - \nu_t)p - 2\nu_t^2 > 0, \\ \text{OR } (2\nu_t + 1)p + \nu_t^2 < 0 \text{ and } (1 - \nu_t)p - 2\nu_t^2 < 0. \end{cases} \quad (29)$$

Now

$$(1 - \nu_t)p - 2\nu_t^2 < 0 \iff \frac{(1 - \nu_t)p}{2} < \nu_t^2. \quad (30)$$

If this holds and $(2\nu_t + 1)p + \nu_t^2 < 0$, it follows that

$$\frac{(1 - \nu_t)p}{2} < -(2\nu_t + 1) \iff \nu_t + 1 < 0, \quad (31)$$

which contradicts the assumption $\nu_t > -1$. Therefore, (27) is equivalent to the conditions

$$(2\nu_t + 1)p + \nu_t^2 > 0, \quad (32a)$$

$$\text{and } (1 - \nu_t)p - 2\nu_t^2 > 0. \quad (32b)$$

The second condition is the same as that obtained in [2, 30]; and it implies that $\nu_t < 1$.

We return to (26) for the discriminant, and by using the expressions of the material parameters

in (20), rewrite this as a function of p as follows:

$$\begin{aligned}
\Delta &= \frac{4E_t^2}{3(1+\nu_t)^2((1-\nu_t)p-2\nu_l^2)^2} \left[(\nu_t^2-1)(2\nu_t+1)p^3 \right. \\
&\quad \left. + \left\{ [4\nu_t^2+6\nu_t+2]\nu_l^2 + [-2\nu_t^2+2]\nu_l - \nu_t^2 + 1 \right\} p^2 + \left\{ [-4\nu_t-4]\nu_l^3 + [-2\nu_t-2]\nu_l^2 \right\} p \right] \\
&= -\frac{4E_t^2}{3(1+\nu_t)^2((1-\nu_t)p-2\nu_l^2)} \left((\nu_t+1)(2\nu_t+1)p^2 - [(2\nu_t+2)\nu_l + \nu_t + 1]p \right) \\
&= -\frac{4E_t^2 p}{3(1+\nu_t)} \frac{(2\nu_t+1)p - (2\nu_l+1)}{(1-\nu_t)p - 2\nu_l^2}.
\end{aligned}$$

From this expression, with (32b), we have $\Delta < 0$ iff

$$(2\nu_t+1)p - (2\nu_l+1) > 0. \quad (33)$$

Furthermore, (33) implies (32a) since

$$0 \leq (\nu_l+1)^2 = \nu_l^2 + 2\nu_l + 1$$

so that

$$2\nu_l + 1 \geq -\nu_l^2. \quad (34)$$

Combining (34) with (33), we obtain (32a).

We summarise as follows: sufficient conditions on the material constants for the elasticity tensor to be pointwise stable are

$$\mu_l \geq \mu_t > 0, \quad p > 0, \quad \nu_t > -1, \quad (35a)$$

$$(2\nu_t+1)p - (2\nu_l+1) > 0, \quad (35b)$$

$$\text{and } (1-\nu_t)p - 2\nu_l^2 > 0. \quad (35c)$$

We illustrate these conditions with some examples.

- (a) Assuming $\nu_l = \nu_t = \nu$, the zones of admissible values of p and ν corresponding to the inequalities (35b) and (35c) are shown in the cross-hatched areas in Figure 1.

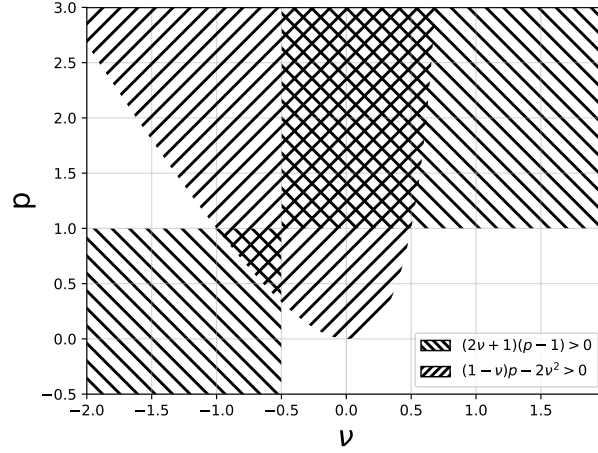


Figure 1: Admissible values for p and ν , according to the inequalities (35b) and (35c)

- (b) If we choose $p = 1$, then (35b) is equivalent to

$$2\nu_t + 1 > 2\nu_l + 1 \iff \nu_t > \nu_l$$

Equation (35c) is equivalent to

$$1 - \nu_t > 2\nu_l^2 \iff |\nu_l| < \sqrt{\frac{1 - \nu_t}{2}}$$

Then, for example, for $\nu_t = 0.5$ we have $-0.5 < \nu_l < 0.5$.

Remarks

1. The expression of Δ is independent of q ; in fact,

$$\beta + 2\gamma = \frac{(1 - \nu_t^2)p^2 + (-2\nu_t\nu_l + 2\nu_t - 2\nu_l - 1)p + 3\nu_l^2}{(1 + \nu_t)((1 - \nu_t)p - 2\nu_l^2)} E_t;$$

thus conditions for pointwise stability hold for any value of $q \geq 1$.

2. For the special case $\nu_t = \nu_l$ and $p = 1$, we have $\beta + 2\gamma = 0$ and $\alpha = 0$, so that

$$\mathcal{A} = \left(\lambda + \frac{2}{3}\mu_t \right) (\text{tr}\boldsymbol{\varepsilon})^2,$$

in which case $\lambda + \frac{2}{3}\mu_t > 0$ is sufficient to ensure $\mathcal{A} > 0$ provided only that $\text{tr}\boldsymbol{\varepsilon} \neq 0$, and therefore $\lambda + \frac{2}{3}\mu_t > 0$ and $\mu_l \geq \mu_t > 0$ would ensure pointwise stability. This includes the case of isotropy, for which $\mu_t = \mu_l$.

3 Governing equations and weak formulation

Consider a transversely isotropic elastic body occupying a bounded domain $\Omega \subset \mathbb{R}^d$, $d = \{2, 3\}$, with boundary $\Gamma = \Gamma_D \cup \Gamma_N$ having exterior unit normal \boldsymbol{n} . Here Γ_D is the Dirichlet boundary, Γ_N the Neumann boundary, and $\Gamma_D \cap \Gamma_N = \emptyset$. The equilibrium equation is

$$-\text{div } \boldsymbol{\sigma}(\boldsymbol{u}) = \boldsymbol{f} \tag{36}$$

and the boundary conditions are

$$\boldsymbol{u} = \boldsymbol{g} \text{ on } \Gamma_D, \tag{37a}$$

$$\boldsymbol{\sigma}(\boldsymbol{u})\boldsymbol{n} = \boldsymbol{h} \text{ on } \Gamma_N. \tag{37b}$$

Here $\boldsymbol{\sigma}$ is the Cauchy stress tensor defined by equation (5), \boldsymbol{u} is the displacement vector, \boldsymbol{f} is the body force, \boldsymbol{g} a prescribed displacement, and \boldsymbol{h} a prescribed surface traction.

We denote by $\mathcal{H}^1(\Omega)$ the Sobolev space of functions which, together with their generalized first derivatives, are square-integrable, and set

$$\mathcal{V} = \{\boldsymbol{u} \in [\mathcal{H}^1(\Omega)]^d; \boldsymbol{u} = \mathbf{0} \text{ on } \Gamma_D\},$$

which is endowed with the norm

$$\|\cdot\|_{\mathcal{V}} = \|\cdot\|_{[\mathcal{H}^1(\Omega)]^d}.$$

We will also use the norm

$$\|\cdot\|_{[\mathcal{L}^2(\Omega)]^d} := \|\cdot\|_0.$$

To take account of the non-homogeneous boundary condition (37a), we define the function $\mathbf{u}_g \in [\mathcal{H}^1(\Omega)]^d$ such that $\mathbf{u}_g = \mathbf{g}$ on Γ_D , and the bilinear form $a(\cdot, \cdot)$ and linear functional $l(\cdot)$ by

$$a : [\mathcal{H}^1(\Omega)]^d \times [\mathcal{H}^1(\Omega)]^d \rightarrow \mathbb{R}, \quad a(\mathbf{u}, \mathbf{v}) = \int_{\Omega} \boldsymbol{\sigma}(\mathbf{u}) : \boldsymbol{\varepsilon}(\mathbf{v}) \, dx, \quad (38a)$$

$$l : [\mathcal{H}^1(\Omega)]^d \rightarrow \mathbb{R}, \quad l(\mathbf{v}) = \int_{\Omega} \mathbf{f} \cdot \mathbf{v} \, dx + \int_{\Gamma_N} \mathbf{h} \cdot \mathbf{v} \, ds - a(\mathbf{u}_g, \mathbf{v}). \quad (38b)$$

The weak form of the problem is then as follows: given $\mathbf{f} \in [\mathcal{L}^2(\Omega)]^d$ and $\mathbf{h} \in [\mathcal{L}^2(\Gamma_N)]^d$, find $\mathbf{U} \in [\mathcal{H}^1(\Omega)]^d$ such that $\mathbf{U} = \mathbf{u} + \mathbf{u}_g$, $\mathbf{u} \in \mathcal{V}$, and

$$a(\mathbf{u}, \mathbf{v}) = l(\mathbf{v}) \quad \forall \mathbf{v} \in \mathcal{V}. \quad (39)$$

We write the bilinear form as

$$a(\mathbf{u}, \mathbf{v}) = a^{iso}(\mathbf{u}, \mathbf{v}) + a^{ti}(\mathbf{u}, \mathbf{v}),$$

where

$$a^{iso}(\mathbf{u}, \mathbf{v}) = \lambda \int_{\Omega} (\nabla \cdot \mathbf{u})(\nabla \cdot \mathbf{v}) \, dx + 2\mu_t \int_{\Omega} \boldsymbol{\varepsilon}(\mathbf{u}) : \boldsymbol{\varepsilon}(\mathbf{v}) \, dx, \quad (40a)$$

$$\begin{aligned} a^{ti}(\mathbf{u}, \mathbf{v}) &= \alpha \int_{\Omega} [(\mathbf{M} : \boldsymbol{\varepsilon}(\mathbf{u}))(\nabla \cdot \mathbf{v}) + (\nabla \cdot \mathbf{u})(\mathbf{M} : \boldsymbol{\varepsilon}(\mathbf{v}))] \, dx + \beta \int_{\Omega} (\mathbf{M} : \boldsymbol{\varepsilon}(\mathbf{u}))(\mathbf{M} : \boldsymbol{\varepsilon}(\mathbf{v})) \, dx \\ &+ \gamma \int_{\Omega} [\boldsymbol{\varepsilon}(\mathbf{u})\mathbf{M} : \boldsymbol{\varepsilon}(\mathbf{v}) + \mathbf{M}\boldsymbol{\varepsilon}(\mathbf{u}) : \boldsymbol{\varepsilon}(\mathbf{v})] \, dx. \end{aligned} \quad (40b)$$

Note that $a^{iso}(\cdot, \cdot)$ and $a^{ti}(\cdot, \cdot)$ are symmetric. The well-posedness of the weak problem requires the bilinear form to be continuous and coercive, and the linear functional continuous.

Assumption. We assume the coefficients in the elasticity tensor \mathbb{C} to satisfy the conditions for pointwise stability given by (35).

Continuity. For all $\mathbf{u}, \mathbf{v} \in \mathcal{V}$, we have

$$\begin{aligned} |a^{iso}(\mathbf{u}, \mathbf{v})| &= \left| \lambda \int_{\Omega} (\nabla \cdot \mathbf{u})(\nabla \cdot \mathbf{v}) \, dx + 2\mu_t \int_{\Omega} \boldsymbol{\varepsilon}(\mathbf{u}) : \boldsymbol{\varepsilon}(\mathbf{v}) \, dx \right| \\ &\leq \max(\lambda, 2\mu_t) \|\mathbf{u}\|_{\mathcal{V}} \|\mathbf{v}\|_{\mathcal{V}}. \end{aligned}$$

Next, we bound the first term on the right-hand side of (40b) as follows:

$$\begin{aligned} \alpha \left| \int_{\Omega} (\mathbf{M} : \boldsymbol{\varepsilon}(\mathbf{u}))(\nabla \cdot \mathbf{v}) \, dx \right| &\leq \alpha \|\mathbf{M} : \boldsymbol{\varepsilon}(\mathbf{u})\|_0 \|\nabla \cdot \mathbf{v}\|_0 \\ &\leq \alpha C_{\alpha} \|\boldsymbol{\varepsilon}(\mathbf{u})\|_0 \|\nabla \cdot \mathbf{v}\|_0 \\ &\leq \alpha C_{\alpha} \|\mathbf{u}\|_{\mathcal{V}} \|\mathbf{v}\|_{\mathcal{V}}. \end{aligned}$$

The other terms are bounded similarly, and we find that a is continuous; that is,

$$|a(\mathbf{u}, \mathbf{v})| \leq M \|\mathbf{u}\|_{\mathcal{V}} \|\mathbf{v}\|_{\mathcal{V}}, \quad (41)$$

where

$$M = C(\max(\lambda, 2\mu_t) + \alpha + \beta + \gamma). \quad (42)$$

Coercivity. For all $\mathbf{v} \in \mathcal{V}$ and $0 \leq k < 1$ we have

$$\begin{aligned} a(\mathbf{v}, \mathbf{v}) &= \int_{\Omega} \boldsymbol{\sigma}(\mathbf{v}) : \boldsymbol{\varepsilon}(\mathbf{v}) \, dx \\ &= \int_{\Omega} \left[\left(\lambda + \frac{2k}{3}\mu_t \right) (\text{tr}\boldsymbol{\varepsilon})^2 + \frac{2}{3}(1-k)\mu_t (\text{tr}\boldsymbol{\varepsilon})^2 + 2\mu_t |\text{dev}\boldsymbol{\varepsilon}|^2 + \beta(\boldsymbol{\varepsilon} : \mathbf{M})^2 + 2\alpha(\text{tr}\boldsymbol{\varepsilon})(\boldsymbol{\varepsilon} : \mathbf{M}) \right. \\ &\quad \left. + 2\gamma(\boldsymbol{\varepsilon} : \boldsymbol{\varepsilon}\mathbf{M}) \right] dx \\ &\geq \int_{\Omega} \left[\left(\lambda + \frac{2}{3}k\mu_t \right) (\text{tr}\boldsymbol{\varepsilon})^2 + \frac{2}{3}(1-k)\mu_t (\text{tr}\boldsymbol{\varepsilon})^2 + (\beta + 2\gamma)(\boldsymbol{\varepsilon}\mathbf{a} \cdot \mathbf{a})^2 + 2\alpha(\text{tr}\boldsymbol{\varepsilon})(\boldsymbol{\varepsilon}\mathbf{a} \cdot \mathbf{a}) \right. \\ &\quad \left. + 2\mu_t |\text{dev}\boldsymbol{\varepsilon}|^2 \right] dx \\ &= \int_{\Omega} \left[\mathcal{A}(k) + \frac{2}{3}(1-k)\mu_t (\text{tr}\boldsymbol{\varepsilon})^2 + 2\mu_t |\text{dev}\boldsymbol{\varepsilon}|^2 \right] dx \end{aligned} \quad (43)$$

where

$$\mathcal{A}(k) = \left(\lambda + \frac{2}{3}k\mu_t \right) (\text{tr}\boldsymbol{\varepsilon})^2 + (\beta + 2\gamma)(\boldsymbol{\varepsilon}\mathbf{a} \cdot \mathbf{a})^2 + 2\alpha(\text{tr}\boldsymbol{\varepsilon})(\boldsymbol{\varepsilon}\mathbf{a} \cdot \mathbf{a}). \quad (44)$$

We note that $\mathcal{A}(1) = \mathcal{A}$ as defined in (25), and thus $\mathcal{A}(1) > 0$ if the conditions (35) are satisfied.

Since $\mathcal{A}(k)$ depends smoothly on k , it follows that $\mathcal{A}(1 - \delta) > 0$ for sufficiently small $\delta > 0$.

Choosing such a δ , and $k = 1 - \delta$ in (43), we obtain

$$\begin{aligned} a(\mathbf{v}, \mathbf{v}) &\geq 2\mu_t \int_{\Omega} (\delta|\text{sph}\boldsymbol{\varepsilon}|^2 + |\text{dev}\boldsymbol{\varepsilon}|^2) dx \\ &\geq K \|\mathbf{v}\|_{\mathcal{V}}^2, \end{aligned} \quad (45)$$

in which $K = 2\delta C\mu_t$, C being a constant arising from Korn's inequality. Hence a is coercive.

Finally we have, using the trace theorem,

$$\begin{aligned} |l(\mathbf{v})| &\leq \|\mathbf{f}\|_0 \|\mathbf{v}\|_0 + \|\mathbf{h}\|_{0,\Gamma_N} \|\mathbf{v}\|_{0,\Gamma} + M \|\mathbf{u}_g\|_{\mathcal{V}} \|\mathbf{v}\|_{\mathcal{V}} \\ &\leq \|\mathbf{f}\|_0 \|\mathbf{v}\|_{\mathcal{V}} + C_0 \|\mathbf{h}\|_{0,\Gamma_N} \|\mathbf{v}\|_{\mathcal{V}} + M \|\mathbf{u}_g\|_{\mathcal{V}} \|\mathbf{v}\|_{\mathcal{V}}, \\ &\leq C \|\mathbf{v}\|_{\mathcal{V}}. \end{aligned}$$

Thus the problem (39) has a unique solution.

4 Conforming finite element approximations

Suppose that Ω is polygonal (in \mathbb{R}^2) or polyhedral (in \mathbb{R}^3), and partitioned into a shape-regular mesh comprising n_e disjoint subdomains Ω_e with boundary $\partial\Omega_e$ and outward unit normal \mathbf{n}_e .

Denote by $\mathcal{T}_h := \{\Omega_e\}_e$ the set of all elements. We define the discrete space $\mathcal{V}^h \subset \mathcal{V}$ by

$$\mathcal{V}^h = \{\mathbf{v}_h \in \mathcal{V} \cap \mathcal{C}(\bar{\Omega}) \mid \mathbf{v}_h|_{\Omega_e} \in [\mathcal{Q}_1(\Omega_e)]^d, \mathbf{v}_h = 0 \text{ on } \Gamma_D\}, \quad (46)$$

where $\mathcal{Q}_1(\Omega_e)$ is the space of polynomials on Ω_e of degree at most 1 in each component.

The discrete problem corresponding to conforming approximations is as follows: find $\mathbf{u}_h \in \mathcal{V}^h$

that satisfies

$$a(\mathbf{u}_h, \mathbf{v}_h) = l(\mathbf{v}_h) \quad \forall \mathbf{v}_h \in \mathcal{V}^h. \quad (47)$$

Since the bilinear form $a(\cdot, \cdot)$ is continuous and coercive and the linear functional $l(\cdot)$ is continuous, from standard finite element convergence theory [31] we have

$$\|\mathbf{u} - \mathbf{u}_h\|_{\mathcal{V}} \leq C_1 h, \quad (48)$$

in which, using (41) and (45), the constant C_1 is given by

$$C_1 = \frac{C(\max(\lambda, 2\mu_t) + \alpha + \beta + \gamma)}{\mu_t}. \quad (49)$$

From (20), all three parameters λ , α , and β have the same denominator $d := (1 + \nu_t)((1 - \nu_t)p - 2\nu_t^2)$. Fixing $\nu_l = \nu_t$ and $q = 1$, for example, we have

$$d(p, \nu_t) = (1 + \nu_t)((1 - \nu_t)p - 2\nu_t^2), \quad (50)$$

which tends to zero as

$$p \rightarrow \frac{2\nu_t^2}{1 - \nu_t}.$$

The limit $p = 1$ corresponds to the case of isotropy, with the well-known limiting value $\nu_t = 1/2$, for which λ becomes unbounded, while $\alpha = \beta = 0$. For anisotropic materials, though, for which $p > 1$, it is seen from (49) and (50) that the constant C_1 in the error bound (48) is bounded, so that in principle one has uniform convergence. This is illustrated in Figure 2, which shows the behaviour of C_1 as a function of p , for near-incompressibility. This issue will be explored later numerically, in Section 5.

4.1 Under-integration

The conforming approximation is known to exhibit volumetric locking while using \mathcal{Q}_1 elements (see for example [26]). To overcome locking, we may under-integrate (i.e. use one-point integration) the terms involving volumetric and extensional deformation. Let \bar{x} be the integration point and

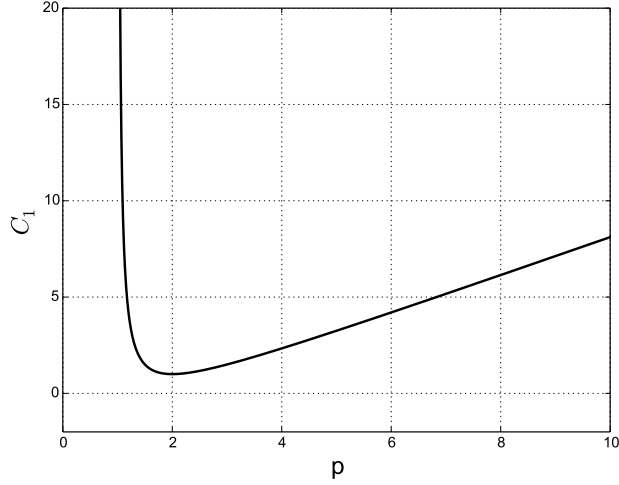


Figure 2: The error bound constant C_1 in (49) against p , with $\nu_l = \nu_t = 0.49995$ and $q = 1$

$\bar{\omega}$ the corresponding weight on element Ω_e .

The volumetric term

$$\lambda \int_{\Omega_e} (\nabla \cdot \mathbf{u}_h)(\nabla \cdot \mathbf{v}_h) dx$$

is then replaced with

$$\lambda(\nabla \cdot \mathbf{u}_h(\bar{\mathbf{x}}))(\nabla \cdot \mathbf{v}_h(\bar{\mathbf{x}}))\bar{\omega}.$$

From (20), we see that α is bounded as $p \rightarrow \infty$ (the inextensional limit), while $\beta \rightarrow \infty$ as $p \rightarrow \infty$.

Thus, in the event of extensional locking with \mathcal{Q}_1 elements, we will replace the extensional term

$$\beta \int_{\Omega_e} (\mathbf{M} : \boldsymbol{\varepsilon}(\mathbf{u}_h))(\mathbf{M} : \boldsymbol{\varepsilon}(\mathbf{v}_h)) dx$$

with

$$\beta \left(\mathbf{M} : \boldsymbol{\varepsilon}(\mathbf{u}_h(\bar{\mathbf{x}})) \right) \left(\mathbf{M} : \boldsymbol{\varepsilon}(\mathbf{v}_h(\bar{\mathbf{x}})) \right) \bar{\omega}.$$

One can easily show that one-point integration is the same as projection of the integrands onto the space of constants. If we define by Π_0 the \mathcal{L}^2 -orthogonal projection onto constants, then under-integrating the volumetric term is the same as replacing it with

$$\lambda \int_{\Omega_e} \Pi_0(\nabla \cdot \mathbf{u}_h) \Pi_0(\nabla \cdot \mathbf{v}_h) dx. \quad (51)$$

Similarly, the extensional term is replaced with

$$\beta \int_{\Omega_e} \Pi_0(\mathbf{M} : \boldsymbol{\varepsilon}(\mathbf{u}_h)) \Pi_0(\mathbf{M} : \boldsymbol{\varepsilon}(\mathbf{v}_h)) dx. \quad (52)$$

Equivalence with perturbed Lagrangian formulation

The perturbed Lagrangian approach takes as a starting point a strain energy of the form

$$W(\boldsymbol{\varepsilon}, T, \beta) = W^{\text{iso}} + T(\boldsymbol{\varepsilon} : \mathbf{M}) - \frac{1}{2\beta} T^2 \quad (53)$$

in which W^{iso} denotes that part of the strain energy that leads to (40a), β now plays the role of a penalty parameter, and T is a Lagrange multiplier. For convenience we assume that $\alpha = 0$ in this section. The stress is obtained from

$$\begin{aligned} \boldsymbol{\sigma} &= \frac{\partial W}{\partial \boldsymbol{\varepsilon}} \\ &= \boldsymbol{\sigma}^{\text{iso}} + T\mathbf{M} \end{aligned} \quad (54)$$

and in addition we have the condition

$$\begin{aligned} 0 &= \frac{\partial W}{\partial T} \\ &= \boldsymbol{\varepsilon} : \mathbf{M} - \frac{T}{\beta}. \end{aligned} \quad (55)$$

We show the equivalence of the perturbed Lagrangian formulation, used for example in [20], to the under-integration formulation (52). In (5) then for $T \in \mathcal{L}^2(\Omega)$ the extensional term in the weak formulation (see (40b)) is

$$\int_{\Omega} T(\mathbf{M} : \boldsymbol{\varepsilon}(\mathbf{v})) dx. \quad (56)$$

With a test function $\vartheta \in \mathcal{L}^2(\Omega)$, we can write the weak form of (55) as

$$\int_{\Omega} \vartheta \left(T - \beta(\mathbf{M} : \boldsymbol{\varepsilon}(\mathbf{u})) \right) dx = 0.$$

The discrete form with $\mathbf{u}_h \in \mathcal{Q}_1(\Omega_e)$ and $T_h, \vartheta_h \in \mathcal{P}_0(\Omega_e)$ at element level is

$$\int_{\Omega_e} \vartheta_h (T_h - \beta(\mathbf{M} : \boldsymbol{\varepsilon}(\mathbf{u}_h))) dx = 0,$$

and since T_h is constant, we have

$$T_h = \frac{\beta}{|\Omega_e|} \int_{\Omega_e} (\mathbf{M} : \boldsymbol{\varepsilon}(\mathbf{u}_h)) dx.$$

We substitute in the discrete form of (56) to obtain

$$\begin{aligned} \int_{\Omega} T_h(\mathbf{M} : \boldsymbol{\varepsilon}(\mathbf{v}_h)) dx &= \sum_{\Omega \in \mathcal{T}_h} \frac{\beta}{|\Omega_e|} \int_{\Omega_e} (\mathbf{M} : \boldsymbol{\varepsilon}(\mathbf{u}_h)) \int_{\Omega_e} (\mathbf{M} : \boldsymbol{\varepsilon}(\mathbf{v}_h)) dx \\ &= \frac{\beta}{|\Omega_e|} \int_{\Omega_e} \Pi_0(\mathbf{M} : \boldsymbol{\varepsilon}(\mathbf{u}_h)) \int_{\Omega_e} \Pi_0(\mathbf{M} : \boldsymbol{\varepsilon}(\mathbf{v}_h)) dx. \end{aligned}$$

Since $\mathbf{M} : \boldsymbol{\varepsilon}(\mathbf{u}_h) \in \mathcal{P}_1(\Omega_e)$, and is integrated exactly using one-point quadrature, this expression is the same as (52), so that the perturbed Lagrangian approximation is equivalent to a mixed $\mathcal{Q}_1 - \mathcal{P}_0(\mathbf{u}_h - T_h)$ formulation, and to under-integration of the extensional term.

5 Numerical tests

In this section, we present the results of numerical simulations of two model problems to illustrate the formulations discussed in the preceding sections. All examples are under conditions of plane strain and based on four- and nine-noded quadrilateral elements with standard bilinear and biquadratic interpolation of the displacement field. Unless otherwise stated, all examples are presented for the case of near-incompressibility, i.e. the value of the transversal Poisson's ratio ν_t is close to 0.5. Precisely, we choose $\nu_t = 0.49995$. We fix the value of the two Poisson's ratios to be equal, and also set $\mu_l = \mu_t$. We consider values of $p > 1$, so that the conditions (35) for pointwise stability are satisfied.

Define $\hat{a} := (\widehat{Ox}, \mathbf{a})$, the angle between the x -axis and the fibre direction \mathbf{a} . For each problem,

the following range of values for \hat{a} will be considered:

$$\hat{a} = \left\{ 0, \frac{\pi}{8}, \frac{\pi}{6}, \frac{\pi}{4}, \frac{\pi}{3}, \frac{3\pi}{8}, \frac{\pi}{2}, \frac{5\pi}{8}, \frac{3\pi}{4}, \frac{7\pi}{8}, \pi \right\}.$$

Recall from Section 4.1 that under-integration is equivalent to a perturbed Lagrangian method.

Also, the standard formulation with large β is equivalent to the penalty formulation as in [20].

The results in the examples that follow are for the following element choices:

- Q_1-CG The standard displacement formulation of order 1
- Q_2-CG The standard displacement formulation of order 2
- $Q_1-CG-UI_\lambda$ The standard displacement formulation with under-integration of the volumetric (λ -) term
- $Q_1-CG-UI_\beta$ The standard displacement formulation with under-integration of the extensional (β -) term
- $Q_1-CG-UI_{\beta\lambda}$ The standard displacement formulation with under-integration of the volumetric and the extensional terms

5.1 Cook's membrane

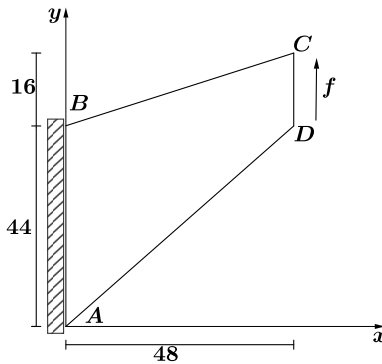
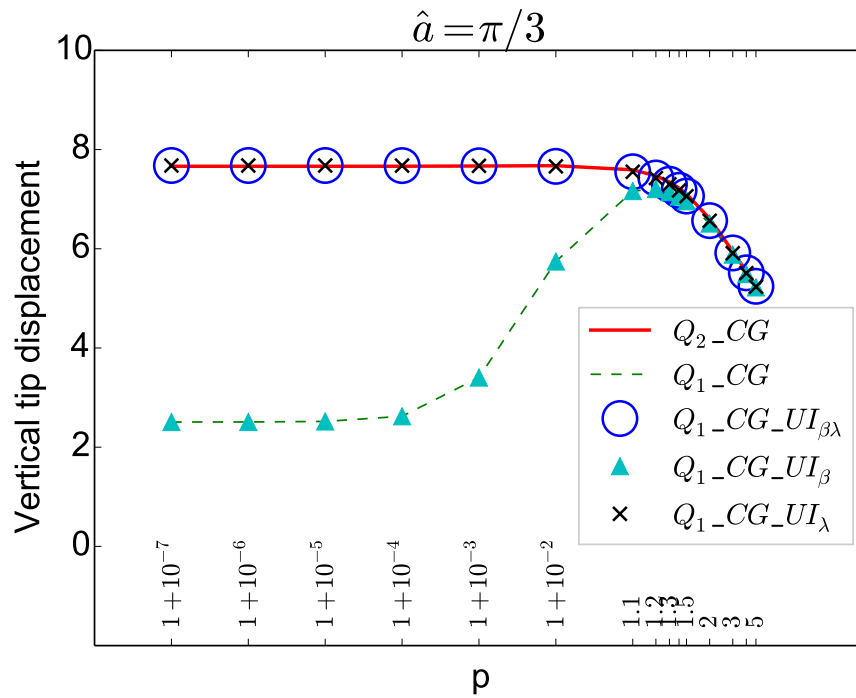
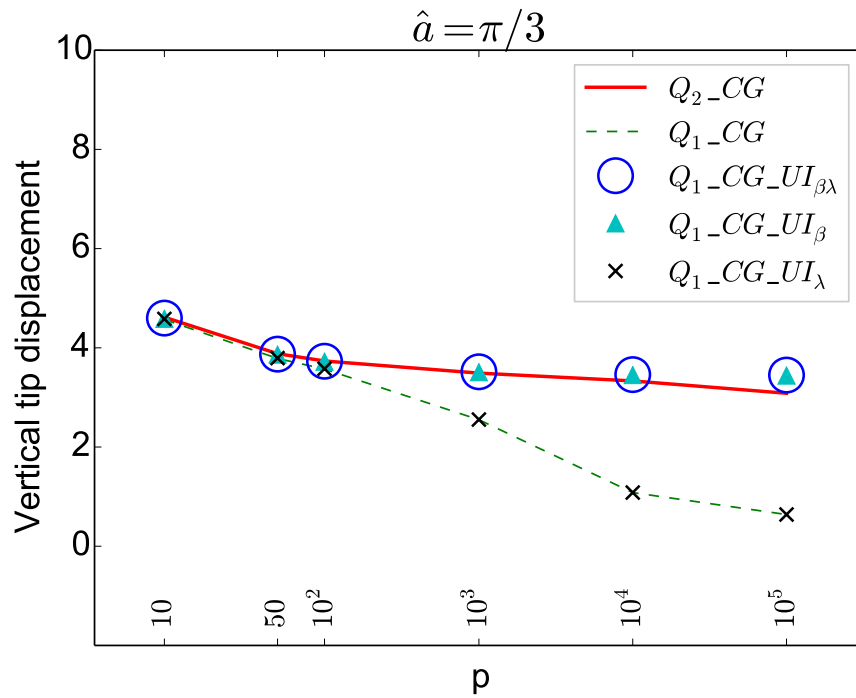


Figure 3: Cook's membrane geometry and boundary conditions

The Cook's membrane test consists of a tapered panel fixed on one edge and subject to a shearing load at the opposite edge as depicted in Figure 3. The applied load is $f = 100$ and $E_t = 250$. This test problem has no analytical solution. The vertical tip displacement at corner C is measured. Figure 4 shows semilog plots of the tip displacement vs p when the fibre direction is at the angle



(a) Moderate values of p



(b) High values of p

Figure 4: Tip displacement vs p for Cook's membrane problem.

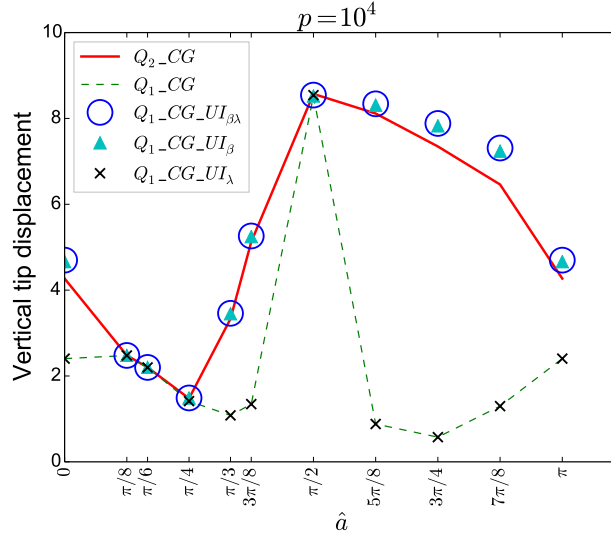


Figure 5: Tip displacement measured at different fibre orientations, for $p = 10^4$

$\pi/3$ for the various element choices. To investigate locking of the proposed formulation, we compare the results with the results obtained using the standard Q_2 -element.

In Figure 4a, for moderate values of p ($1 \leq p \leq 5$) the Q_1-CG formulation behaves well away from $p = 1$, with evidence of locking behaviour as $p \rightarrow 1$. Locking is avoided when the volumetric term is under-integrated ($Q_1-CG-UI_{\lambda}$). Notice that for $Q_1-CG-UI_{\beta}$ there is still locking, as the locking is purely volumetric. In Figure 4b, for higher values of p ($10 \leq p \leq 10^5$), the Q_1-CG method shows locking behaviour as p get bigger, and convergent behaviour with $Q_1-CG-UI_{\beta}$. Notice that under-integrating only the volumetric term ($Q_1-CG-UI_{\lambda}$) has no effect since the locking is purely extensional. $Q_1-CG-UI_{\beta\lambda}$ shows locking-free behaviour everywhere. Figure 5 shows tip displacements for various fibre orientations, where the degree of anisotropy is fixed at $p = 10^4$. The behaviour observed in Figure 4 is evident here over the range of fibre directions.

5.2 Bending of a beam

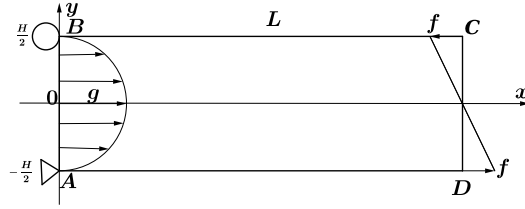


Figure 6: Beam geometry and boundary conditions

We consider the beam shown in Figure 6, subject to a linearly varying load along the edge CD. The horizontal displacement u is constrained at node B, while the node A is constrained in both directions. The beam has length $L = 10$ and height $H = 2$ and the applied load has a maximum value $f = 3000$. Here, $E_t = 1500$. The boundary conditions are

$$\begin{cases} u(0, y) = g(y), \\ v(0, -\frac{H}{2}) = 0, \end{cases}$$

where

$$g(y) = -\frac{f}{H} \mathfrak{S}_{31} \left(y^2 - \frac{H^2}{4} \right).$$

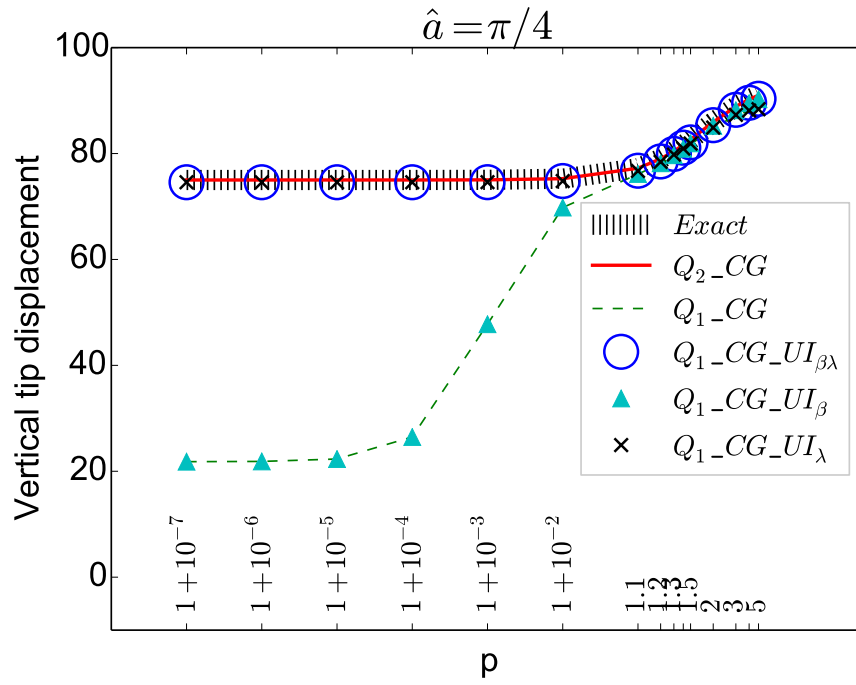
The compliance coefficients \mathfrak{S}_{ij} are given in the Appendix. The analytical solution is

$$\begin{cases} u(x, y) = -\frac{2f}{H} \left(\mathfrak{S}_{11}xy + \frac{1}{2}\mathfrak{S}_{31} \left(y^2 - \frac{H^2}{4} \right) \right), \\ v(x, y) = -\frac{f}{H} \left(\mathfrak{S}_{21} \left(y^2 - \frac{H^2}{4} \right) - \mathfrak{S}_{11}x^2 \right). \end{cases}$$

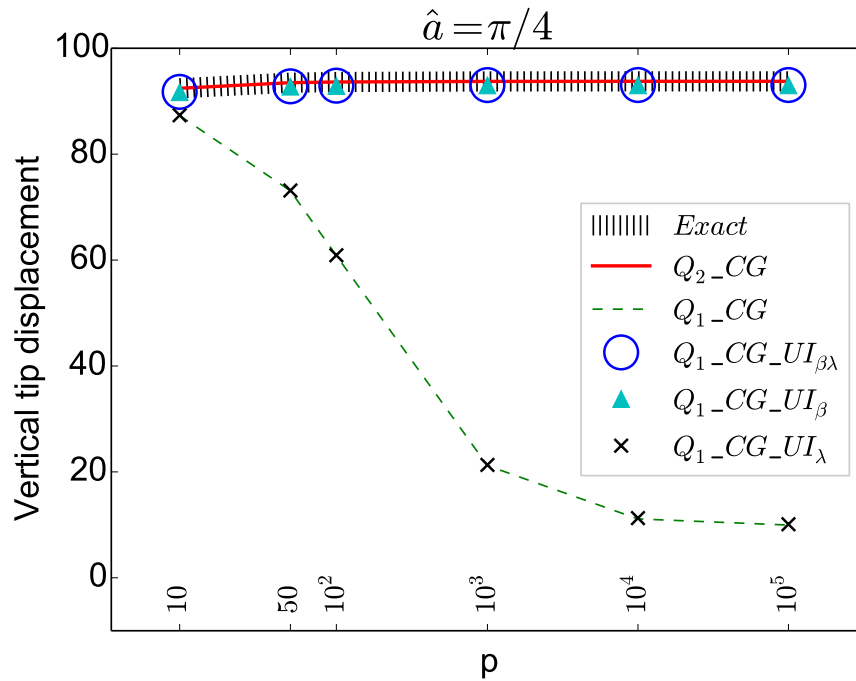
The linearly varying load \hat{f} with maximum f is

$$\hat{f}(y) = -\frac{2f}{H}y.$$

In Figure 7, which shows semilog plots of tip displacement for different values of p , with the angle of the fibre direction $\pi/4$, locking behaviour is investigated by comparison with the analytical solution. The same behaviour as appears for the Cook's example is seen, i.e. for moderate



(a) Moderate values of p



(b) High values of p

Figure 7: Tip displacement vs p for the beam problem

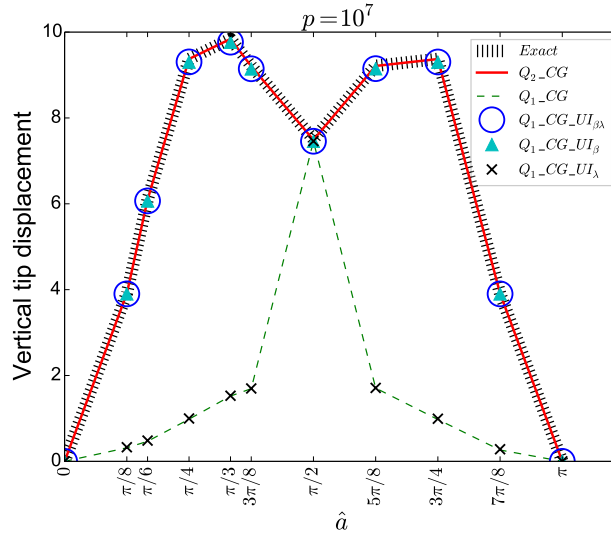


Figure 8: Tip displacement measured at different fibre orientations

values of p away from $p = 1$ (approximately, $1.1 \leq p \leq 5$), there is locking-free behaviour with Q_1-CG , while locking occurs as p approaches 1. This is overcome by using under-integration ($Q_1-CG-UI_{\lambda}$) (Figure 7a). For high values of p there is purely extensional locking with Q_1-CG , which is overcome by using $Q_1-CG-UI_{\beta}$ (Figure 7b). $Q_1-CG-UI_{\beta\lambda}$ shows locking-free behaviour for any value of p . Figure 8 shows tip displacements for various fibre orientations where the degree of anisotropy is fixed at $p = 10^7$. Extensional locking of Q_1-CG is observed except for the angles $0, \pi/2$. For the angle $0 (= \pi)$, the material is very stiff, relative to the type of loading. For the angle $\pi/2$ no locking is observed. This can be accounted for by two factors: first, with this orientation the property of near-inextensibility in the vertical direction has a negligible effect on the bending-dominated deformation; and secondly, as previously discussed, the presence of anisotropy serves to circumvent volumetric locking.

The following set of results show behaviour for various fibre orientations, and for values of $p = 1.0001, 3$ and 10^4 .

Figure 9 shows the \mathcal{H}^1 -error convergence plots for all the formulations considered for $p = 1.0001$. Here $Q_1-CG-UI_{\lambda}$ and $Q_1-CG-UI_{\beta\lambda}$ show optimal convergence for any fibre direction at the superlinear rate 1.83. Q_1-CG and $Q_1-CG-UI_{\beta}$ show poor convergence. Figure 10 shows the \mathcal{H}^1 -error convergence plots for all the formulations considered for $p = 3$. Here, all formulations

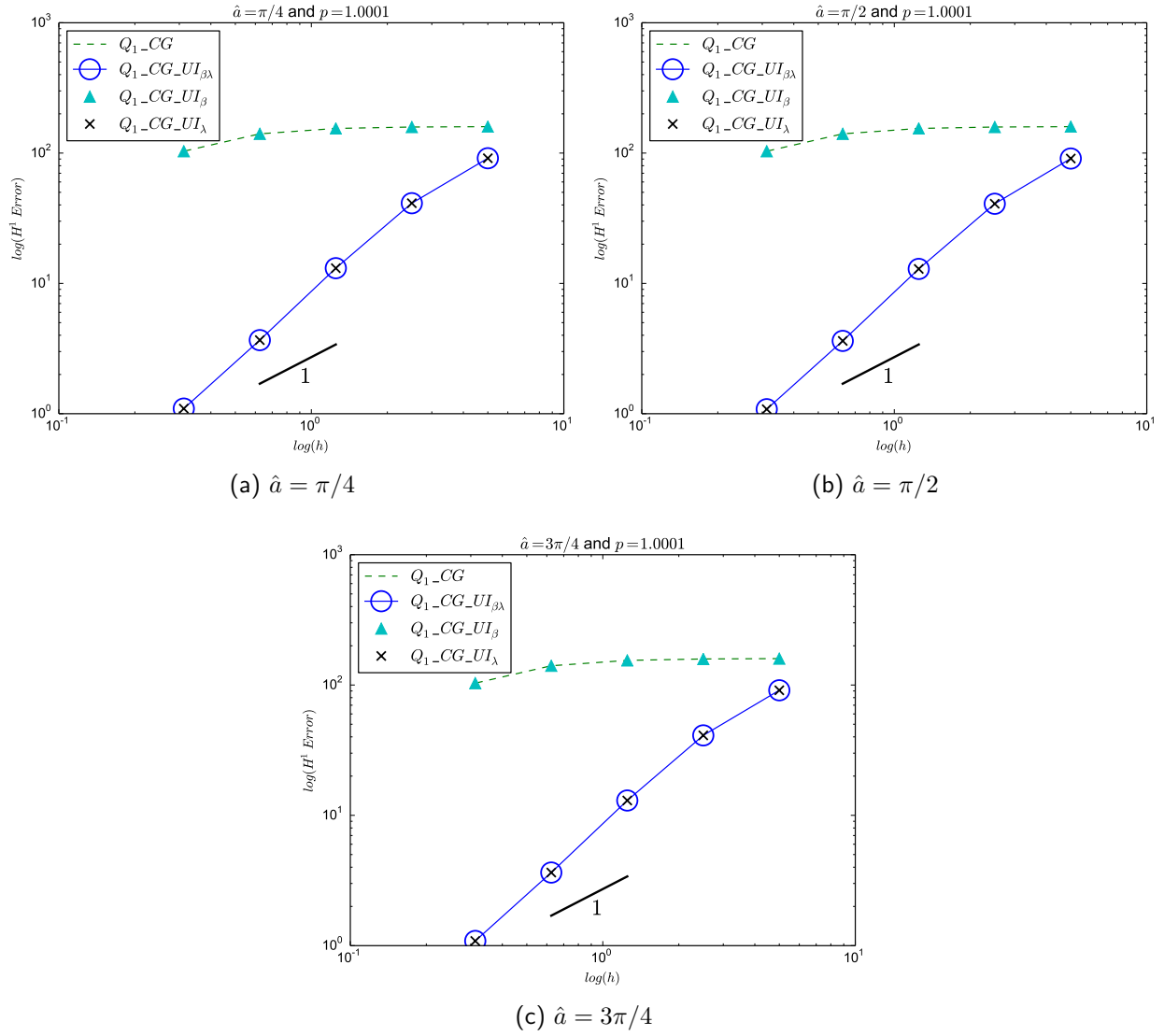


Figure 9: Comparison of \mathcal{H}^1 errors for conforming and under-integrated elements on quadrilaterals, for different fibre orientations, and for $p = 1.0001$

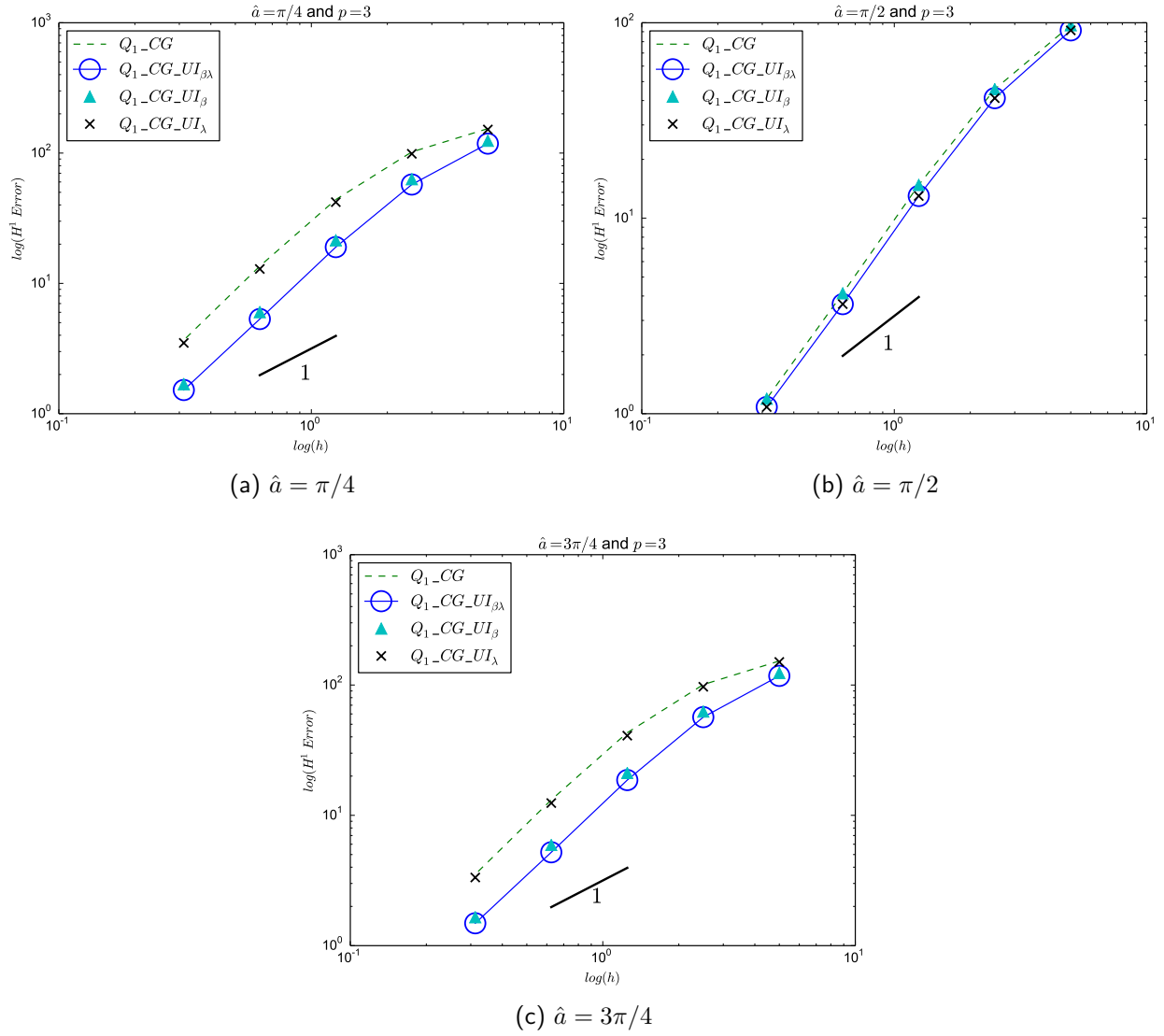


Figure 10: Comparison of \mathcal{H}^1 errors for conforming and under-integrated elements on quadrilaterals, for different fibre orientations, and for $p = 3$

at any fibre direction are superlinearly convergent at rate 1.7. Figure 11 shows the \mathcal{H}^1 -error convergence plots for all the formulations considered, for $p = 10^4$. Figure 11a and Figure 11c show optimal convergence at the rate 1.86 for $Q_1-CG-UI_\beta$ and $Q_1-CG-UI_{\beta\lambda}$, and poor convergence for Q_1-CG and $Q_1-CG-UI_\lambda$. In Figure 11b where the fibre direction is at an angle $\pi/2$, the error plots show convergence at the superlinear rate 1.64 for Q_1-CG .

6 Conclusions

The results in this work shed useful light on the relationship between well-posedness and anisotropy in the context of transverse isotropy, and show that, as far as computational approximations are concerned, transverse isotropy can have the effect of eliminating volumetric locking behaviour for moderate values of the anisotropy parameter, but away from its value of unity which would correspond to isotropy. The use of under-integration in the extensional term follows the well-established approach used to circumvent volumetric locking; an extensive set of numerical results, over a range of measures of anisotropy and a range of fibre directions, has shown in this work that under-integration is robustly locking-free.

The study and development of finite element formulations for incompressible and near-incompressible behaviour is extensive, with rigorous analyses supporting a range of stable and convergent element choices, whether with the use of mixed and enhanced formulations, equivalent under-integration schemes, or discontinuous Galerkin approaches, to mention some examples. A corresponding framework is lacking in the case of near-inextensibility. The work reported here is intended to contribute to that framework. Further investigations will involve the analysis and implementation of mixed and discontinuous Galerkin formulations.

There have been a substantial number of investigations of near-inextensible behaviour under large-strain conditions. It is clear from these studies, which were referred to in the Introduction, that the large-deformation problem presents features and challenges, some of which are absent in the small-strain regime. It is intended to build on these investigations and the work reported here, in exploring theoretically and computationally the large-deformation problem.

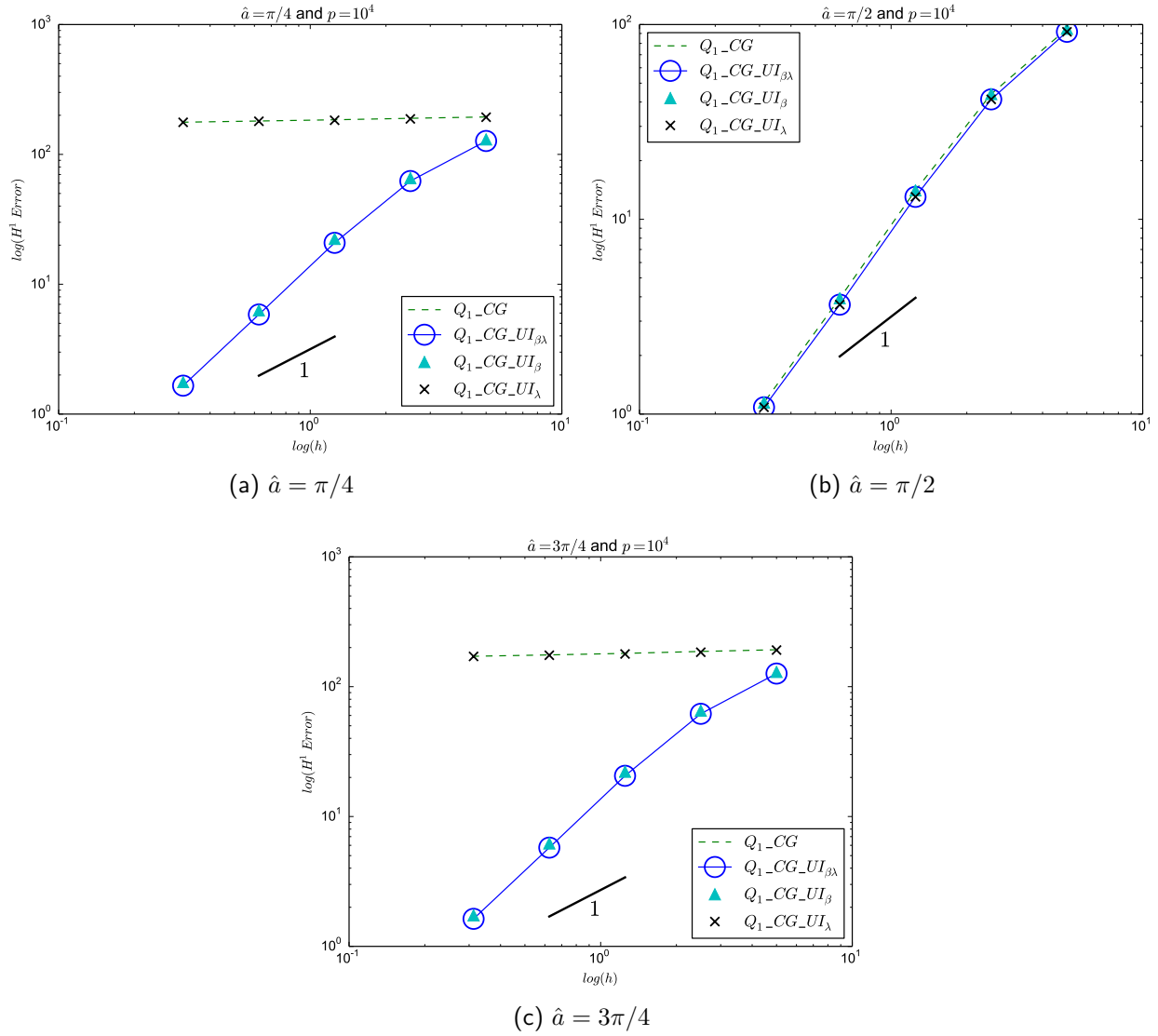


Figure 11: Comparison of \mathcal{H}^1 errors for conforming and under-integrated elements on quadrilaterals, for different fibre orientations, and for $p = 10^4$

Appendix

For plane strain, the strain-stress relationship for a transversely isotropic material, with fibre direction $\mathbf{a} = \begin{pmatrix} a_1 \\ a_2 \end{pmatrix}$, is

$$\begin{pmatrix} \varepsilon_{11} \\ \varepsilon_{22} \\ 2\varepsilon_{12} \end{pmatrix} = \begin{pmatrix} \mathbb{S}_{11} & \mathbb{S}_{12} & \mathbb{S}_{13} \\ \mathbb{S}_{12} & \mathbb{S}_{22} & \mathbb{S}_{23} \\ \mathbb{S}_{13} & \mathbb{S}_{23} & \mathbb{S}_{33} \end{pmatrix} \begin{pmatrix} \sigma_{11} \\ \sigma_{22} \\ \sigma_{12} \end{pmatrix},$$

where

$$\begin{aligned} \mathbb{S}_{11} &= \frac{1}{\det\mathbb{C}} \left[(\lambda + 2\mu_t + 2(\gamma + \alpha)a_2^2 + \beta a_2^4) \left(\mu_t + \frac{\gamma}{2} + \beta a_1^2 a_2^2 \right) - ((\alpha + \gamma)a_1 a_2 + \beta a_1 a_2^3)^2 \right] \\ \mathbb{S}_{12} &= \frac{1}{\det\mathbb{C}} \left[((\alpha + \gamma)a_1 a_2 + \beta a_1^3 a_2) ((\alpha + \gamma)a_1 a_2 + \beta a_1 a_2^3) - (\lambda + \alpha + \beta a_1^2 a_2^2) \left(\mu_t + \frac{\gamma}{2} + \beta a_1^2 a_2^2 \right) \right] \\ \mathbb{S}_{13} &= \frac{1}{\det\mathbb{C}} \left[(\lambda + \alpha + \beta a_1^2 a_2^2) ((\alpha + \gamma)a_1 a_2 + \beta a_1 a_2^3) - ((\alpha + \gamma)a_1 a_2 + \beta a_1^3 a_2) (\lambda + 2\mu_t + 2(\gamma + \alpha)a_2^2 + \beta a_2^4) \right] \\ \mathbb{S}_{22} &= \frac{1}{\det\mathbb{C}} \left[(\lambda + 2\mu_t + 2(\gamma + \alpha)a_1^2 + \beta a_1^4) \left(\mu_t + \frac{\gamma}{2} + \beta a_1^2 a_2^2 \right) - ((\alpha + \gamma)a_1 a_2 + \beta a_1^3 a_2)^2 \right] \\ \mathbb{S}_{23} &= \frac{1}{\det\mathbb{C}} \left[(\lambda + \alpha + \beta a_1^2 a_2^2) ((\alpha + \gamma)a_1 a_2 + \beta a_1^3 a_2) - (\lambda + 2\mu_t + 2(\gamma + \alpha)a_1^2 + \beta a_1^4) ((\alpha + \gamma)a_1 a_2 + \beta a_1 a_2^3) \right] \\ \mathbb{S}_{33} &= \frac{1}{\det\mathbb{C}} \left[(\lambda + 2\mu_t + 2(\gamma + \alpha)a_1^2 + \beta a_1^4) (\lambda + 2\mu_t + 2(\gamma + \alpha)a_2^2 + \beta a_2^4) - (\lambda + \alpha + \beta a_1^2 a_2^2)^2 \right] \end{aligned}$$

with

$$\begin{aligned} \frac{1}{\det\mathbb{C}} &= (\lambda + 2\mu_t + 2(\gamma + \alpha)a_1^2 + \beta a_1^4) \left[(\lambda + 2\mu_t + 2(\gamma + \alpha)a_2^2 + \beta a_2^4) \left(\mu_t + \frac{\gamma}{2} + \beta a_1^2 a_2^2 \right) \right. \\ &\quad \left. - ((\alpha + \gamma)a_1 a_2 + \beta a_1 a_2^3)^2 \right] \\ &\quad - (\lambda + \alpha + \beta a_1^2 a_2^2) \left[(\lambda + \alpha + \beta a_1^2 a_2^2) \left(\mu_t + \frac{\gamma}{2} + \beta a_1^2 a_2^2 \right) \right. \\ &\quad \left. - ((\alpha + \gamma)a_1 a_2 + \beta a_1^3 a_2) ((\alpha + \gamma)a_1 a_2 + \beta a_1 a_2^3) \right] \\ &\quad + ((\alpha + \gamma)a_1 a_2 + \beta a_1^3 a_2) \left[(\lambda + \alpha + \beta a_1^2 a_2^2) ((\alpha + \gamma)a_1 a_2 + \beta a_1 a_2^3) \right. \\ &\quad \left. - ((\alpha + \gamma)a_1 a_2 + \beta a_1^3 a_2) (\lambda + 2\mu_t + 2(\gamma + \alpha)a_2^2 + \beta a_2^4) \right]. \end{aligned}$$

Acknowledgements

The authors acknowledge with thanks the support for this work by the National Research Foundation, through the South African Research Chair in Computational Mechanics.

References

- [1] H. Altenbach. Modelling of anisotropic behavior in fiber and particle reinforced composites. In T. Sadowski, editor, *Multiscale Modelling of Damage and Fracture Processes in Composite Materials*, pages 1–62. Springer, 2005.
- [2] G.E. Exadaktylos. On the constraints and relations of elastic constants of transversely isotropic geomaterials. *International Journal of Rock Mechanics and Mining Sciences*, 38(7):941–956, 2001.
- [3] J. Humphrey. *Cardiovascular Solid Mechanics: Cells, Tissues and Organs*. Springer, New York, 2002.
- [4] R.W. Ogden. *Non-linear Elastic Deformations*. Ellis Horwood Ltd., Chichester, 1984.
- [5] Z. Hashin. Theory of composite materials. In Z. Hashin and C.T. Herakovich, editors, *Mechanics of Composite Materials*, pages 201–242. Pergamon Press, 1970.
- [6] A.C. Pipkin. Stress analysis for fiber-reinforced materials. *Advances in Applied Mechanics*, 19:1–51, 1979.
- [7] A.J.M. Spencer. *Deformations of Fibre-reinforced Materials*. Clarendon Press, Oxford, 1972.
- [8] T.C. Ting. *Anisotropic Elasticity: Theory and Applications*. Oxford University Press, 1996.
- [9] M. Hayes and C.O. Horgan. On the displacement boundary-value problem for inextensible elastic materials. *The Quarterly Journal of Mechanics and Applied Mathematics*, 27(3):287–297, 1974.

- [10] M. Hayes and C.O. Horgan. On mixed boundary-value problems for inextensible elastic materials. *Zeitschrift für Angewandte Mathematik und Physik ZAMP*, 26(3):261–272, 1975.
- [11] J. Schröder and P. Neff. Invariant formulation of hyperelastic transverse isotropy based on polyconvex free energy functions. *International Journal of Solids and Structures*, 40(2):401–445, 2003.
- [12] J. Schröder, P. Neff, and D. Balzani. A variational approach for materially stable anisotropic hyperelasticity. *International Journal of Solids and Structures*, 42(15):4352–4371, 2005.
- [13] J.A. Weiss, B.N. Maker, and S. Govindjee. Finite element implementation of incompressible, transversely isotropic hyperelasticity. *Computer Methods in Applied Mechanics and Engineering*, 135(1-2):107–128, 1996.
- [14] A. Zdunek, W. Rachowicz, and T. Eriksson. A five-field finite element formulation for nearly inextensible and nearly incompressible finite hyperelasticity. *Computers & Mathematics with Applications*, 72(1):25–47, 2016.
- [15] A. Zdunek and W. Rachowicz. A 3-field formulation for strongly transversely isotropic compressible finite hyperelasticity. *Computer Methods in Applied Mechanics and Engineering*, 315:478–500, 2017.
- [16] A. Zdunek and W. Rachowicz. A mixed higher order fem for fully coupled compressible transversely isotropic finite hyperelasticity. *Computers & Mathematics with Applications*, 74(7):1727–1750, 2017.
- [17] P. Wriggers, J. Schröder, and F. Auricchio. Finite element formulations for large strain anisotropic material with inextensible fibers. *Advanced Modeling and Simulation in Engineering Sciences*, 3(1):25, 2016.
- [18] C.Ó. Brádaigh and R.B. Pipes. A finite element formulation for highly anisotropic incompressible elastic solids. *International Journal for Numerical Methods in Engineering*, 33(8):1573–1596, 1992.

- [19] P. Wriggers, B. Hudobivnik, and J. Korelc. Efficient low order virtual elements for anisotropic materials at finite strains. In E. Oñate, D. Peric, E. de Souza Neto, and M. Chiumenti, editors, *Advances in Computational Plasticity*, pages 417–434. Springer, 2018.
- [20] F. Auricchio, G. Scalet, and P. Wriggers. Fiber-reinforced materials: finite elements for the treatment of the inextensibility constraint. *Computational Mechanics*, 60(6):905–922, 2017.
- [21] M. Zeidi and C.I.L. Kim. Mechanics of an elastic solid reinforced with bidirectional fiber in finite plane elastostatics: complete analysis. *Continuum Mechanics and Thermodynamics*, 30(3):573–592, 2018.
- [22] M. Zeidi and C.I.L. Kim. Mechanics of fiber composites with fibers resistant to extension and flexure. *Mathematics and Mechanics of Solids*, <https://doi.org/10.7939/R3Z892V17>, 2017.
- [23] D.J. Steigmann. Theory of elastic solids reinforced with fibers resistant to extension, flexure and twist. *International Journal of Non-Linear Mechanics*, 47(7):734–742, 2012.
- [24] D.N. Arnold and R.S. Falk. Well-posedness of the fundamental boundary value problems for constrained anisotropic elastic materials. *Archive for Rational Mechanics and Analysis*, 98(2):143–165, 1987.
- [25] M.J.H. Dantas. On the boundary value problems of linear elasticity with constraints. *Journal of Elasticity*, 54(2):93–111, 1999.
- [26] T.J.R. Hughes. *The Finite Element Method: Linear Static and Dynamic Finite Element Analysis*. Prentice-Hall, Inc., 1987.
- [27] V. Lubarda and M. Chen. On the elastic moduli and compliances of transversely isotropic and orthotropic materials. *Journal of Mechanics of Materials and Structures*, 3(1):153–171, 2008.
- [28] A.J.M. Spencer. The formulation of constitutive equation for anisotropic solids. In J.P. Boehler, editor, *Mechanical Behavior of Anisotropic Solids/Comportment Mécanique des Solides Anisotropes*, pages 3–26. Springer, Dordrecht, 1982.

- [29] J.E. Marsden and T.J.R. Hughes. *Mathematical Foundations of Elasticity*. Prentice-Hall, Inc, Englewood Cliffs, 1983.
- [30] W.M. Lai, D.H. Rubin, and E. Krempl. *Introduction to Continuum Mechanics*. Butterworth-Heinemann, 2009.
- [31] P. G. Ciarlet. *The Finite Element Method for Elliptic Problems*. North-Holland, Amsterdam, 1978.